Presented at 5th International
Conference on High-Energy Physics
and Nuclear Structure, Uppsala,
Sweden, June 18-22, 1973

LBL-2052

HIGH-ENERGY HEAVY IONS: A NEW AREA FOR PHYSICS RESEARCH

Harry H. Heckman

June 15, 1973

Prepared for the U.S. Atomic Energy Commission
under Contract W-7405-ENG-48

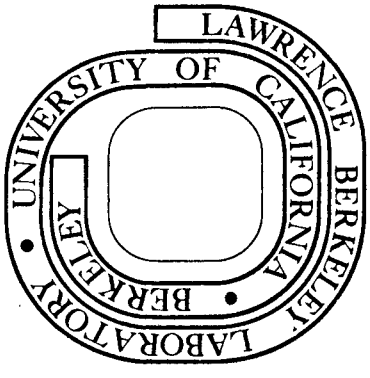

LBL-2052

DISCLAIMER

HIGH-ENERGY HEAVY IONS: A NEW AREA FOR PHYSICS RESEARCH

Harry H. Heckman
Lawrence Berkeley Laboratory
University of California
Berkeley, California 94720

ABSTRACT

Emerging from the first heavy ion experiments at the Bevatron are preliminary results that reveal high-energy heavy ion research to be a promising and stimulating new area of physics research, pertinent to elementary particles, nuclear structure, and cosmic rays. Amongst the heavy ion physics experiments in progress at the Bevatron are studies on the fragmentation of projectile and target nuclei, coherent pion production and the production and detection of high-energy hypernuclei. The experiments on the fragmentation of beam nuclei at 1.05 and 2.1 GeV/nucleon have shown specific relevance to contemporary theory on inclusive reactions, particularly to the concept of factorization, i.e., the modes of fragmentation of beam nuclei are independent of the target nucleus. Complementary experiments on the fragmentation of target nuclei are concerned with the characteristic differences between the production of light and heavy fragments from heavy element targets under bombardment by p, ^{12}C, and ^{16}O beams at 2.1 GeV/nucleon. The investigation on the feasibility of producing high-energy hyperfragments, via the two-body reaction $^{A}Z + p \rightarrow {}^{A+1}Z_{\Lambda} + K^{+}$, where the target proton and heavy ion projectile become, respectively, a K^{+} and a high velocity hyperfragment, may lead to a new technique in the field of hypernuclear physics.

HIGH-ENERGY HEAVY IONS: A NEW AREA FOR PHYSICS RESEARCH

The physics of high energy heavy ions, after its dramatic beginnings less than two years ago[1,2], is rapidly approaching maturity, becoming one of the most exhilirating and promising areas of Bevatron research. Since the first high-energy heavy-ion beams were accelerated in the Bevatron in August, 1971, all ions with charge : mass ratio Z/A = 1/2, ^{2}H through ^{20}Ne, have been accelerated and extracted at energies 0.250 to 2.1 GeV/nucleon. During the past year a development and improvement program has resulted in increased heavy-ion beam intensities and has provided for versatile beam control and monitoring. Table I gives typical beam intensities now in current use at the Bevatron.

The immediate demand for experimental beam time has given support to the contention that the availability of relativistic beams of heavy ions at the Bevatron provides the experimenter with a new and here-to-fore unavailable tool for physics research. One of the most attractive features of high-energy heavy-ion research is that it encomposses a broad range of multidisciplinary research in the fields of high energy physics, nuclear structure, cosmic rays and biomedical research.

To give an overall impression of the multidisciplinary nature of the heavy ion program at the Bevatron, I list in Table II a representative sample of physics experiments that are in progress or have been completed. From this list I have selected several experiments for further discussion---experiments that have produced preliminary results of significant interest ---certain to influence the directions for future heavy ion research.

Contrasts in the Production of He and Be Fragments from Heavy Target Nuclei by Protons and Heavy Ions at 2.1 GeV/nucleon*

J. Sullivan, University of California
H. Crawford
P. B. Price

During the past decade experimental studies on the fragments ejected from complex target nuclei in high energy proton collisions have supplied much of our present information on the basic characteristics of the fragmentation process[3]. In the low-energy region, nuclear evaporation models have been particularly successful in explaining spectra at 90^{o} to the incident beam, provided one specifies that the isotopic fragment emission takes place from a set of moving nuclei with a Maxwellian distribution of excitation energies and forward momenta. Satisfactory agreement with experiment is attained, however, only when the Coulomb barrier is taken to be about 0.4 of the classical tangent spheres barrier. The intensity of the fragments in the forward direction is much higher than can be accounted for by the evaporation models, hence, must originate in the high-energy cascade.

The goals of Sullivan, et al in their first heavy ion experiments were to search for new models of nuclear disintigration (such as shock waves), look for multiple fragment emission in the forward hemisphere, and to compare the fragmentation spectra from Au and U targets produced by incident p and ^{16}O beams at 2.1 GeV/nucleon.[4] The principal innovation in their experiment is the use of Lexan polycarbonate detectors, for by employing a three stage (etch + UV + re-etch) processing, they obtain charge identification for $Z \geq 6$.

* Supported by the U.S. Atomic Energy Commission

Figure 1 shows the configuration of one of their experimental designs to study the energy (0.1 to 20 MeV/nucleon) and angular distribution (15^{o} to 60^{o} and 120^{o} to 165^{o}) of fragments $Z \geq 2$ produced in 50μ thick Au and U targets bombarded by p, ^{12}C and ^{16}O beams at 2.1 GeV/nucleon. In Figure 2 the spectra of ^{4}He from the reaction ^{16}O(2.1 GeV/n) + Au is compared with that produced by the proton (5.5 GeV) bombardment of Au.[3] Although the angles of emissions are not the same, the qualitative features of the comparison is that, in ^{16}O collisions, the Coulomb barrier is further suppressed and the multiplicity of ^{4}He emission is about twice as large as that in proton collisions. Figure 3 presents preliminary data on the energy spectra and angular distribution of Be nuclei emitted from the ^{12}C (2.1 GeV/n) + U interaction. The data are compared with the ^{4}He spectra from the 5.5 GeV proton data of Korteling, et al.[3]

From a series of such measurements as illustrated in Figures 2 and 3, Sullivan, et al have arrived at the following conclusions:

a) On comparing heavy ion (^{12}C and ^{16}O) with proton collisions, they find:
   1) more energy is deposited in the nucleus by heavy ions,
   2) the yield of $6 \leq Z \leq 15$ and $1 \leq E \leq 5$ MeV/nucleon is $\sim$ 10 x greater for heavy ions, and
   3) $\langle Z \rangle$, $\langle E \rangle$, and E_{min} of the fragments are smaller.

b) $\sigma(Z>6) > \sigma$ geometric $\approx$ 4b.

c) Coulomb barrier is < 1/3 the hard sphere barrier,

d) Multiple heavy ion emission (up to 3) occurs for Z>6 fragments, a lower limit since only forward hemisphere has been examined, and

e) There is no evidence for shock waves, i.e., no preferential angles of emission.

Production of Hypernuclei in a 2.1 GeV/nucleon Oxygen Beam*

T. Bowen, University of Arizona
G. Cable
D. A. Delise
E. W. Jenkins
R. M. Kalbach
K. J. Nield
R. C. Noggle
A. E. Pifer

Since relativistic hypernuclei might travel many centimeters in the laboratory before decaying, they could escape from thick production targets and their lifetimes readily observed. Relativistic velocities also would facilitate measuring the Z of the hypernucleus and the decay products would be confined to small laboratory solid angles suitable for momentum analysis.

A search has been made by the University of Arizona group for relativistic hypernuclei associated with the production of low momentum K^+ mesons which provide an electronic signature by their delayed decay after stopping. A wide-gap spark chamber was photographed each time a possible K^+ -decay was detected, indicative of the two-body hypernucleus production reaction $^{16}O + p \rightarrow {}^{+}K + {}^{17}O_{\Lambda}$. In this reaction the target proton converts to a K^+ meson, which can be emitted near 90° in the laboratory, while the 2.1 GeV/nucleon ^{16}O ion proceeds as a relativistic hyperfragment. Figure 4 shows the experimental arrangement. The K^+ decays were detected by delayed coincidence D_1D_2 or U_1U_2. The photographs of the wide-gap spark chamber were scanned for tracks which appeared to originate from decay vertices outside the target.

The histogram of the distances of the vertex points from the center of the 7.5 cm thick polyethylene production target is shown in Figure 5[a].

---

* Supported by the National Science Foundation

The large peaks at 20 and 50 cm are attributable to nuclear interactions in the 0.025 mm Al spark chamber plates and the 0.75 mm scintillation counter B3. Clearly, many of the events with vertex positions outside the plates must also be nuclear interactions. In order to separate many of these from hypernuclear decay events, the distribution of the number of forward prongs was examined for several subgroups of events, as shown in Figure 6. The interactions in the scintillation counter and first plate had the broad prong distribution shown in Figure 6[a]. The events with vertices within the first spark chamber gap are shown in Figure 6[b]. Finally, presumably the purest sample of hypernuclear decay events, those with vertices between the production target and the spark chamber, are shown in Figure 6[c]. This latter distribution appears appreciably narrower than for known nuclear interactions in Figure 6[a], as expected for the comparatively small energy release in hypernuclear decay. On this basis, only events outside of plates with 2, 3, or 4 forward prongs were further considered. The decay distance distribution of these events is shown in Figure 5[b]. This distribution, and the associated K^+ decay-time distribution for these events, are both consistent with attributing these particular events to the production and decay of hypernuclei.

Assuming these events are hypernuclei, the cross section per target nucleon for 2.1 GeV/nucleon ^{16}O bombarding CH in our geometry, which requires $P_{lab}(K^+) \lesssim 400$ MeV/C, is of the order of 0.12 ± 0.03 μb/nucleon (the indicated error is statistical only). Since the present arrangement yielded roughly one relativistic hypernucleus per hour of running, further optimization of the geometry and triggering scheme will be necessary before it will be practical to study hypernuclear properties with this technique.

Particle Production and Fragmentation : Interactions of Relativistic Protons, Deuterons and Alpha Particles With Be, C, Cu and Pb Targets*

J. Jaros, Lawrence Berkeley Laboratory
J. Papp
L. Schroeder
J. Staples
H. Steiner
A. Wagner

This experiment represents the first major effort of a general survey of the production of light positive and negative particles from the bombardment of various targets by p, d, and, ^{4}He at kinetic energies 1.05 and 2.1 GeV/nucleon. Reported here are some of the results derived from a study of particle production at a laboratory angle of 2.5° to the incident beam. The main features of the experiment are:

a) Projectiles: p, d, α

b) Energies: 1.05 GeV/nucleon p, d, α
2.1 GeV/nucleon p, d, α
4.2 GeV p

c) Targets : Be, C, Cu, Pb

d) Secondary particles detected : $\pi^{\pm}$, K^{+}, $p^{\pm}$, d, ^{3}H, He^3, He^4

e) Rigidity of Secondaries: $0.5 \leq p/z \leq 4.5$ Gev/c

f) Resolution of magnetic spectrometer : $\Delta p/p \approx 1\%$

g) Particle Identification : Momentum, time-of-flight, $\frac{dE}{dx}$

Initial results of particular interest derived from this experiment are in the areas of pion production and the fragmentation of deutrons and alpha particles by target nuclei Be, C, Cu and Pb. Presented in Figure 7 are the spectra of negative pions produced at 2.5° by protons, deuterons, and alpha particles at 2.1 GeV/nucleon in a carbon target. A single nucleon at 2.1 GeV energy cannot produce pions with momentum greater than about 2 GeV/C. However, Jaros, et al. have observed

* Supported by the U. S. Atomic Energy Commission

significant production of pions with momentum greater than 2 GeV/C when deuterons and alphas at E = 2.1 GeV/nucleon interact with the target nuclei. The shape of the observed pion spectra cannot be reproduced by a model in which the production is attributed solely to single collisions between individual nucleons inside the projectile and target nucleus, (unless rather pathological, non-physical, momentum distributions are assumed for the nucleons inside the projectiles). Either multiple scattering terms or other types of coherent mechanisms in which more than a single projectile nucleon is involved seem to be necessary to explain the observed spectra.

Additional results on pion production have led to the following conclusions:

a) Preliminary results with positive pions are in accord with the negative pion results.
b) No breakdown of charge independence has been observed in $\pi^{\pm}$ production by deuterons and alpha particles on carbon.
c) The shape of the production spectrum for high energy pions (above $\approx$ 1 GeV) is independent of the atomic mass number A of the target.

Figures 8 and 9 give the target dependence for the production of π^- mesons by 2.1 GeV/nucleon alpha particles, as a function of the momentum of the produced pion. For momenta $p_\pi \gtrsim 1.0$ GeV/C, the production cross sections vary as $A_{target}^{1/3}$ with impressive precision. As the momentum of the π^- decreases, the target dependence tends to change, from what can be classically characterized as a peripheral interaction, to one that varies $\approx A^{1/2}$, suggesting that an $A^{2/3}$ (geometrical) cross section may become important at low π^- momenta. Figure 10 gives the momentum/charge spectra of secondary particles p, d, and ^{3}He produced by the fragmentation of ^{4}He nuclei, E = 1.05 GeV/n, in C and Cu targets.

Also illustrated is the elastically scattered alpha peak from the Cu target. The arrows indicate the momentum/charge that corresponds to the velocity of the incident beam. The shape of the momentum distributions of these high energy fragments from alpha, as well as deuteron collisions with various targets is independent of target material, as displayed by the C and Cu data in Figure 10. The results indicate that deuteron and ^{3}He production from alpha particles are, respectively, about equal to, and 1/2 of, the production of protons at the 2.5^o production angle.

The objective of these experiments is to provide information about nucleon correlations inside alpha particles, nuclear clustering, and the momentum distribution of these clusters. Measurements of the proton momentum distributions can be used directly, in conjuction with measured proton-nucleus pion production cross sections, to estimate more realistically pion production in deuteron and alpha particle collisions with nuclei, as described previously.

Many of the concepts presently used in high energy elementary particle interactions, e.g. scaling, limiting fragmentation, parton structure, find direct applicability in this type of experiment. In a certain sense, heavy ion interactions at Bevatron energies may be closer to asymptopia than similar types of "elementary particle" experiments performed at ISR and NAL energies.

Heavy Ion Fragmentation of ^{16}O Nuclei at 2.1 GeV/nucleon*

H. H. Heckman, Lawrence Berkeley Laboratory
G. E. Greiner, University of California, Space Sciences Laboratory
P. J. Lindstrom
F. S. Bieser

The experiment on the fragmentation of ^{16}O nuclei by Heckman, et al continue and extend earlier work on the 0^{o}- fragmentation of ^{14}N beam nuclei at 2.1 GeV/nucleon.[5] The first experimental results gave evidence that the single particle inclusive spectra are independent of the target nucleus. Another striking feature of the fragmentation process is that, within the measurement error, the forward going fragments of the beam projectile have mean velocities equal to the velocity of the incident beam. It is this last property that has proven extremely useful in the production of well defined secondary beams of isotopes.

Figure 11 is a scale drawing of the 0^{o} heavy-ion magnetic spectrometer that has been designed and brought into operation to carry out the 0^{o}-fragmentation experiments. The spectrometer focuses magnetically analysed beam fragments, produced within 12.5 mr of the beam direction, onto charge-measuring solid-state detector telescopes placed along the focal plane of the spectrometor. The rigidity $R(GV/c) = p/z$ of the fragments is given by the expression $R = K(D)/D$, where D is the deflection distance and K(D) is a slowly varying function of D. Salient features of the isotopic identification are:

i) Rigidity resolution (rms)
$\Delta R/R = 0.6\ \Delta D/D \quad (130 \leq D \leq 400cm)$

ii) Charge resolution (rms)
$\Delta Z = \pm 0.1e$

iii) Time of flight (FWHM)
$\Delta t = 100$ psec

* Supported by the U. S. Atomic Energy Commission and National Aeronautics and Space Administration

Because the beam fragments have well defined velocities, the magnetic spectrometer effectively becomes a Z/A ($\propto$D) spectrometer. How the isotopes are spatial separated along the guide rail is illustrated in Figure 12 where the distance D is indicated for all isotopes with $A \leq 16$. Figure 13 presents the measured spectrum of the carbon isotopes as a function of D produced by the fragmentation of ^{16}O beam nuclei at E = 2.1 GeV/nucleon in a beryllium target. If we now take the N(D) spectrum and express it in terms of longitudinal momentum, we obtain the distribution $N(p_{\parallel})$ shown in Figure 14. Qualitative properties of the carbon spectrum are:

i) the peak intensity occurs at A = 12,
ii) the envelope of the spectrum diminishes monotonically as $|A - 12|$ increases, and
iii) the spectral shape in momentum space of the various isotopes are the same.

To the accuracy of the measurements, a characteristic of all such spectra, helium through oxygen, is that the maximum for each isotope occurs at a momentum corresponding to the beam velocity.

The curves drawn through the individual carbon isotope spectra are Gaussian functions of momentum $P_{\parallel}$, all having equal standard deviations. When these distributions are transformed to the projectile frame (where the beam projectile is at rest), the momentum distribution conduce to a single (Gaussian) distribution of form $N(P_{\parallel})_{proj} \propto \exp[-P^2_{\parallel}/2(m_{\pi}c)^2]$. This is illustrated in Figure 15 where we have plotted the longitudinal momentum distributions $N(P_{\parallel})$ versus $P_{\parallel}$ for a sample of isotopes of the elements Z = 1 to 8 produced by the fragmentation of ^{16}O nuclei (Be target) at 2.1 GeV/nucleon. (The sample was selected on a criterion of minimal statistical accuracy for the spectrum of each isotope.) Within the indicated typical error, the distributions $N(P_{\parallel})$ are remarkably consistent with a

unique Gaussian function with $\sigma = m_\pi c = 140$ MeV/C.

To complement these longitudinal momenta data, we present in Figures 16[a, b, c] our first measurements of transverse momenta. These distributions were derived from the analysis of particle trajectories using a pair of 3-plane (120^o) multiwire chambers (128 wires, 1 mm wire spacing) placed behind the detector telescopes. The data presented for ^{15}N, ^{14}C and ^{13}C are the projected transverse momentum distributions $N(P_\perp)$ as measured. Both x- and y- components of $P_\perp$, normal to, and in the plane of the spectrometer, were measured and are shown in the figure ($P_\parallel$ is along the z-axis). We anticipate that uncertainties in the incident beam direction, multiple scattering in the target and spatial resolution of the wire chambers will affect a 5 - 10% correction to the standard deviations of the $N(P_\perp)$ spectra.

As was done for the longitudinal momentum distributions given in Figure 15, we compare the perpendicular momentum distributions for ^{15}N, ^{14}C and ^{13}C to Gaussian functions. The solid curve has a standard deviation $\sigma = 140$ MeV/C, the dashed curves --- 100 and 180 MeV/c. The hash-marks in the vicinity of 500 MeV/c in each figure indicate the maximum value of $P_\perp$ that is transmitted by the spectrometer system for the laboratory momentum of each isotope. These $P_\perp$ (max) correspond to a 12.5 mrad production angle at the target. Although the data are preliminary, they clearly indicate that no significant differences are apparent between the longitudinal and transverse momentum distributions. Both can be characterized by Gaussian functions with widths $\sigma \approx m_\pi c$. In Figure 16[c], we have included the longitudinal momentum distribution for ^{13}C(see Figure 15) to exhibit the similarity between the parallel and perpendicular momentum distributions.

At this stage, the experimental results strongly suggest that, in the projectile frame, the longitudinal and transverse momentum distributions of the fragmentation products of heavy ion beams at 2.1 GeV/nucleon are the same, with a characteristic width approximately $m_\pi c$.

Furthermore, these distributions appear to be independent of the atomic mass of the fragment.

That the fragmentation of relativistic heavy ions via the nucleus-nucleus interaction proceeds with a minimal value of momentum transfer suggests that theories pertaining to single particle inclusive spectra, may be applicable to heavy ion fragmentations. Of immediate relevancy is the concept of the factorization of cross-sections. Factorization states that in the reaction A + B → X + ----, the partial cross sections factor according to the rule $\sigma_{AB}^{X} \rightarrow \gamma_A^X \gamma_B$ where the function $\gamma^X(A)$ depends on the beam nucleus A and its fragmentation product X and γ_B is a function of the target nucleus B only.

As previously mentioned, the first high energy fragmentation experiments performed at the Bevatron gave evidence for such factorization, i.e., the modes of fragmentation are independent of the target nucleus.

In a conventional transmission experiment, we have measured the total cross sections for the production of B, C, and N from ^{16}O ions and B from ^{12}C ions at E = 2.1 GeV/nucleon in targets of CH_2, C, S, Cu and Pb. In this experiment, only the initial (Z = 6 or 8) and final (effective) charge Z^* of the products were measured. Figure 17 is a plot of the target factor γ_B, versus the mass of the target. If it is assumed that γ_B is of the form $\gamma_B = M^n$, where M is in atomic mass units, then γ_A^X is equal to the total cross section for the production of X from beam nucleus A in hydrogen. With a fitted target factor exponent of n = 0.256, the factorable cross section becomes $\sigma_{AB}^X = \sigma_A^X M^{0.256}$, an expression that fits the data to a confidence level of 0.6

REFERENCES

1. White, M. G., Isaila, M., Prelec, K., Allen, H. L., Science, 174, 1121 (1971).

2. Grunder, H. A., Hartsough, W. O., Lofgren, E. J., Science, 174, 1128 (1971).

3. Korteling, R. G., Toren, C. R., and Hyde, E. K., Energy Spectra of Fragments from Silver and Uranium Bombarded with 5.0 GeV Protons, LBL Report 663, August 1972.

4. Sullivan, J., Price, P. B., Crawford, H. J., Whitehead, M., Phys. Rev. Lett., 30, 136 (1973).

5. Heckman, H. H., Greiner, D. E., Lindstrom, P. J., and Bieser, F. S., Phys. Rev. Lett., 28 926 (1972).

TABLE I

PRESENT INTENSITY WITH 20 MEV PROTON LINAC

ION	Charge State in Linac	(Particles per Pulse on Target)
^{1}H	+1	$> 10^{12}$
^{2}H	+1	2×10^{11}
^{3}He	+1	10^{11}
^{4}He	+2	2×10^{10}
^{12}C	+4	1×10^{8}
^{14}N	+5	1×10^{7}
^{16}O	+5	1.5×10^{7}
^{20}Ne	+6	10^{5}

TABLE II

CURRENT HEAVY ION PHYSICS RESEARCH PROGRAM AT BEVATRON

- Heavy Ion Fragmentation: Single Particle Inclusion Spectra at Forward Angles
- Heavy Ion Total Cross-Section Measurements
- Range and Ionization Studies
- Positive and Negative Particle Production: Search for Coherent Pion Production
- Nuclear Fragmentation of Heavy Target Nuclei Induced by High Energy Heavy Ions
- d-p Backward Elastic Scattering
- Production and Study of a Tagged, Mono-energetic Neutron Beam
- Production of High Energy Hypernuclei
- Emulsion Studies of Target Fragmentation, Spallation and Heavy Ion Cross Sections
- Calibration of Particle Detection and Identification Systems for Satellite and Balloon Flight Experiments

FIGURE CAPTIONS

Fig. 1 Configuration of target and Lexon detectors for low energy fragmentation experiments.

Fig. 2 Energy spectra of ^{4}He produced at 40^{o} by ^{16}O bombardment of Au and by 5.5 GeV proton bombardment of U, ref. 3.

Fig. 3 Relative spectral shapes of Be production in heavy target under ^{12}C (2.1 GeV/n) and proton (5.5 GeV) bombardment, ref. 3.

Fig. 4 Experimental configuration for the detection of high energy hypernuclei.

Fig. 5 a) Distribution of the origins of all candidates for hypernuclear decays.

b) Same as a) but limited to 2-4 prong events in forward hemisphere.

Fig. 6 Prong distribution for three sub-groups of events a) in chamber plate, b) in gas of chamber, and c) between target and chamber.

Fig. 7 π^{-} production by 2.1 GeV/n p, d, and α beams, carbon target.

Fig. 8 Target dependence of π^{-} production by 2.1 GeV/nucleon alpha particles. Pion momenta 1.25 to 2.5 GeV/c.

Fig. 9 Target dependence of π^{-} production by 2.1 GeV/nucleon alpha particles. Pion momenta 0.5 to 1.0 GeV/c.

Fig. 10 Yields of p, ^{3}He and d at 2.5^{o}(lab) from the fragmentation of 1.05 GeV/n alpha particles in C and Cu targets. The ^{4}He elastically scattered peak is also shown.

Fig. 11 Magnetic spectrometer for the 0^{o}-fragmentation experiment. Fragments of heavy ion beam (^{16}O) produced within 12.5 mr of the beam direction are focused along guide rail according to charge and momentum.

Fig. 12 Deflection distance D vs Z and A of isotopes produced at 0^{o} and at beam velocity.

Fig. 13 Observed count-rate versus D of the carbon isotopes produced by the fragmentation of ^{16}O nuclei at 2.1 GeV/nucleon.

Fig. 14 Momentum spectrum for the carbon isotopes produced by the fragmentation of ^{16}O nuclei at 2.1 GeV/nucleon.

Fig. 15 Longitudinal momentum distributions in projectile frame.

Fig. 16 Transverse momentum distributions for a) ^{15}N, b) ^{14}C and c) ^{13}C isotopes produced by fragmentation of ^{16}O fragmentation at 2.1 GeV/nucleon. Transverse components in, and normal to, the plane of the magnetic spectrometer are shown. The longitudinal momentum spectrum for ^{13}C is also shown for comparison in c).

Fig. 17 Target factor $\gamma(B)$ versus M(amu) of target, the solid line denoted $\gamma(B) = M^{0.256}$.

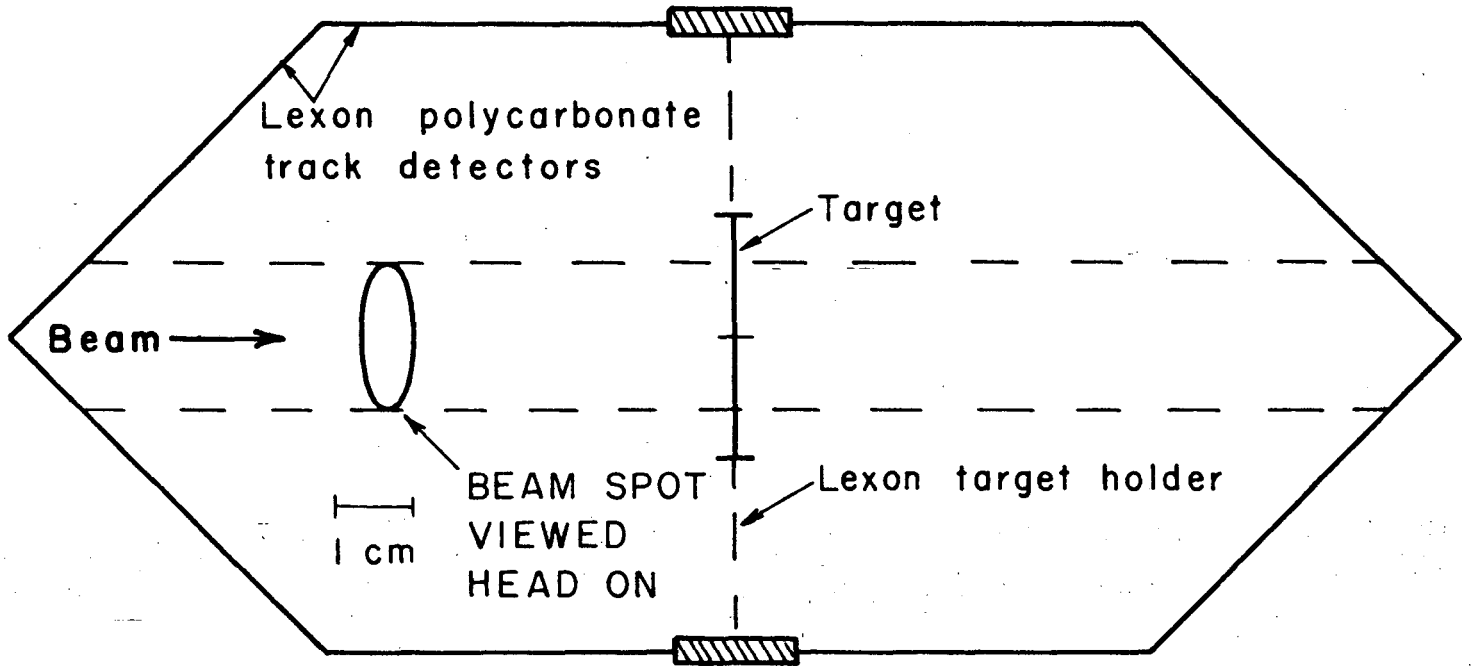
Lexon polycarbonate
track detectors
Target
Beam
BEAM SPOT
VIEWED
HEAD ON
1 cm
Lexon target holder

Fig. 1

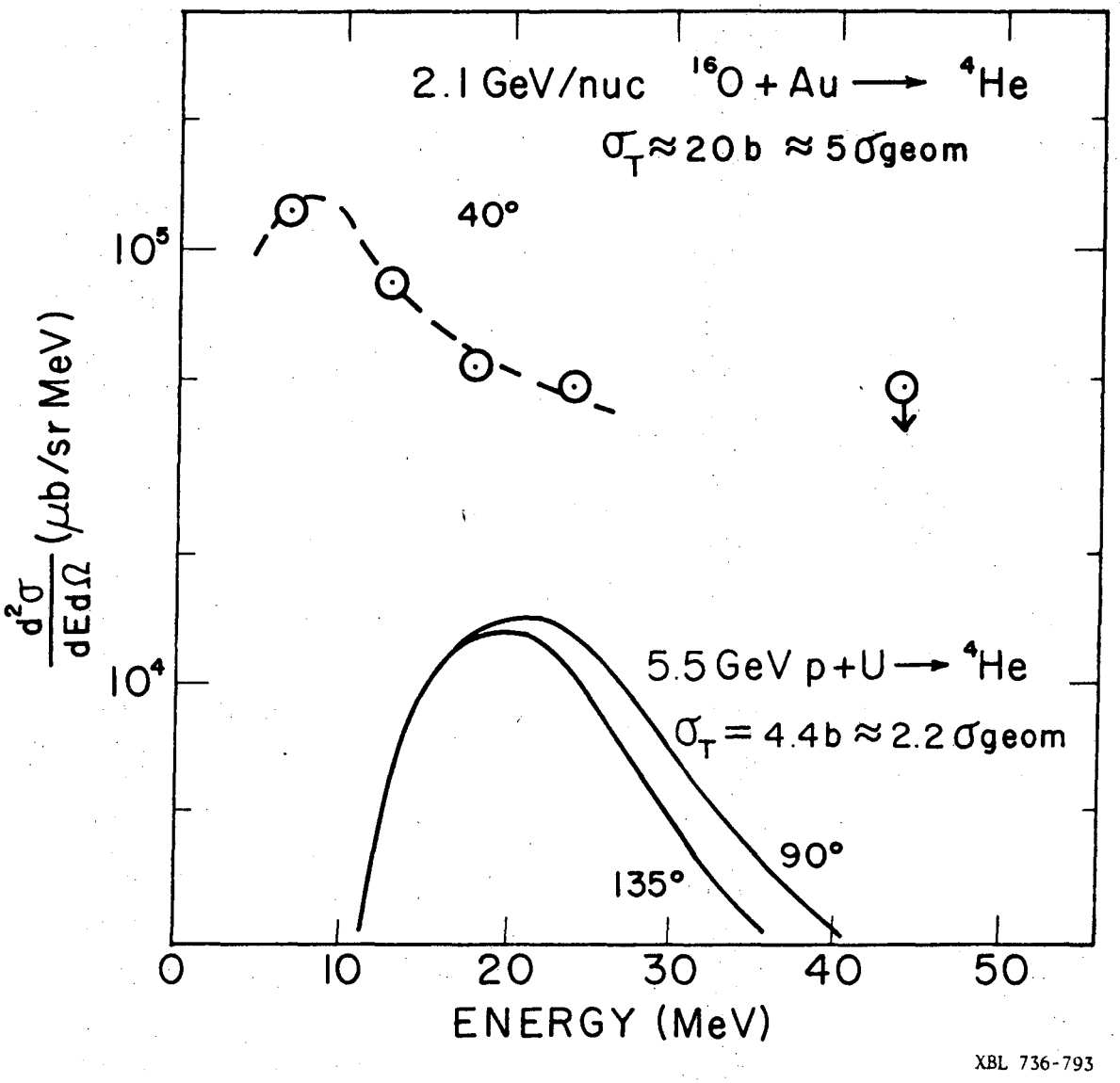
2.1 GeV/nuc $^{16}O + Au \longrightarrow {}^{4}He$
$\sigma_T \approx 20\,b \approx 5\,\sigma_{geom}$
40°
10^5
$\frac{d^2\sigma}{dE\,d\Omega}$ (μb/sr MeV)
5.5 GeV p+U $\longrightarrow {}^{4}He$
$\sigma_T = 4.4\,b \approx 2.2\,\sigma_{geom}$
10^4
90°
135°
0
10
20
30
40
50
ENERGY (MeV)
XBL 736-793

Fig. 2

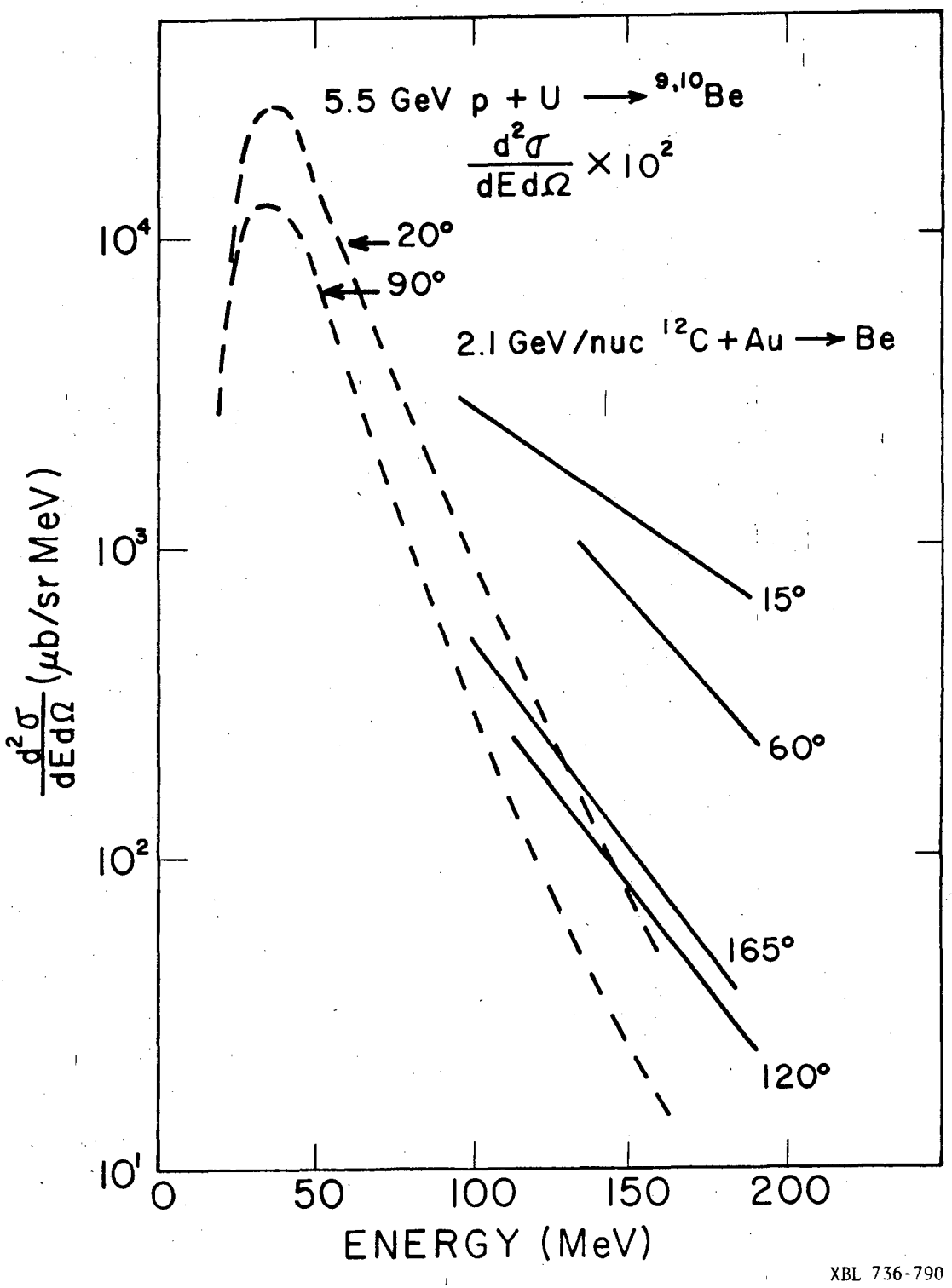
5.5 GeV p + U → 9,10Be
d²σ/dEdΩ × 10²
20°
90°
2.1 GeV/nuc 12C + Au → Be
15°
60°
165°
120°
d²σ/dEdΩ (μb/sr MeV)
10⁴
10³
10²
10¹
0
50
100
150
200
ENERGY (MeV)
XBL 736-790

Fig. 3

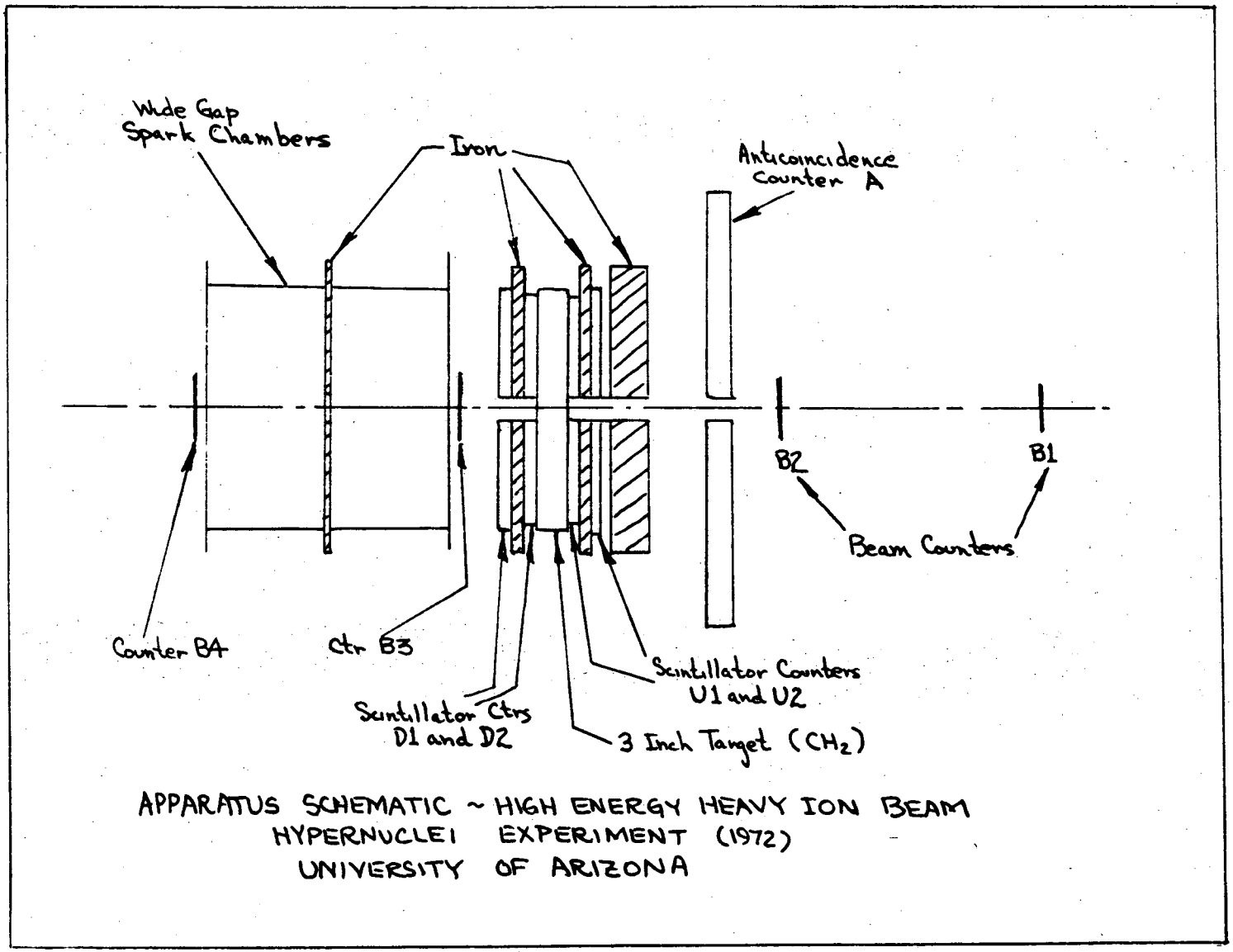

APPARATUS SCHEMATIC ~ HIGH ENERGY HEAVY ION BEAM
HYPERNUCLEI EXPERIMENT (1972)
UNIVERSITY OF ARIZONA

XBL 736-796

Fig. 4

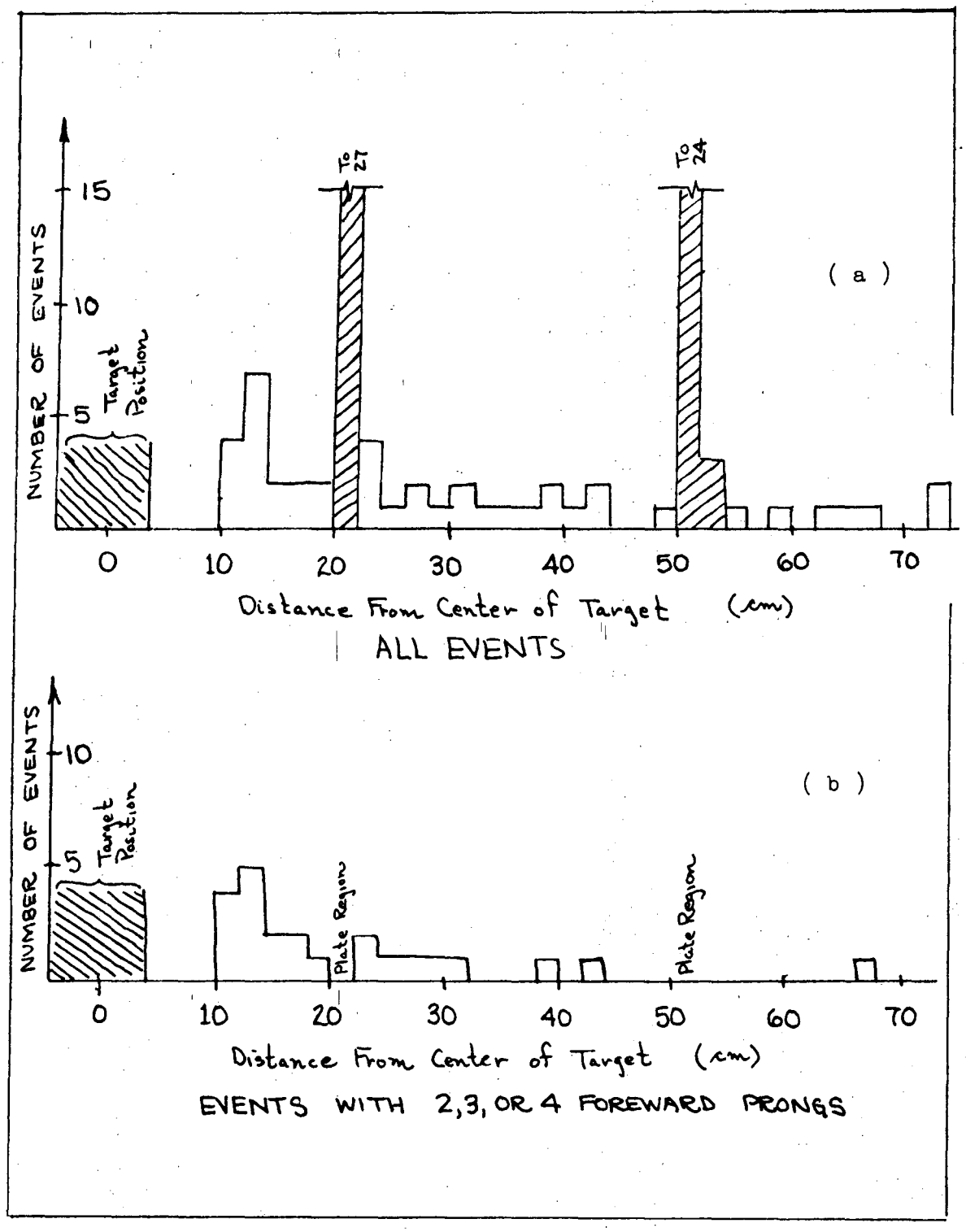

XBL 736-789

Fig. 5

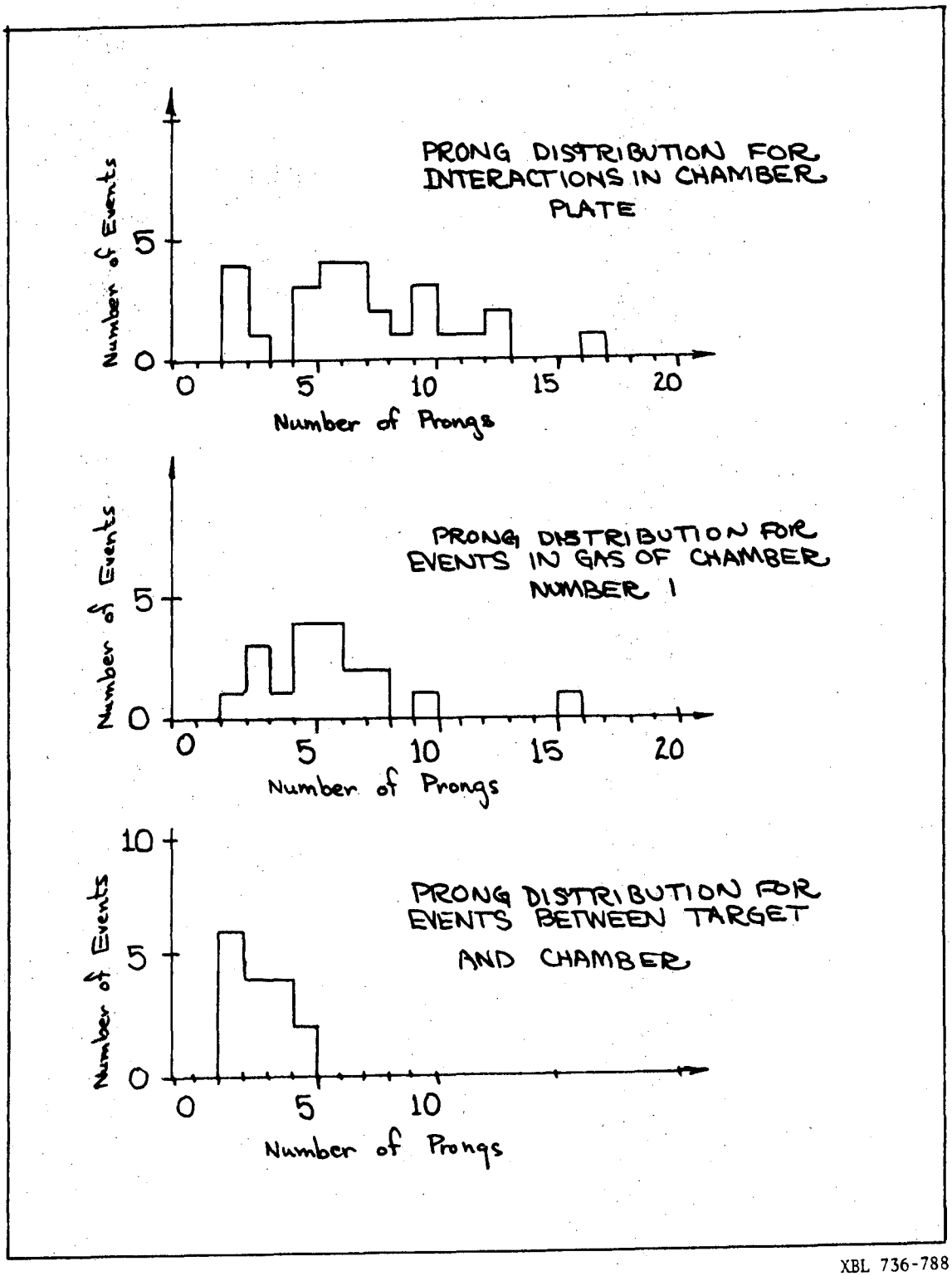
PRONG DISTRIBUTION FOR INTERACTIONS IN CHAMBER PLATE
Number of Events
0
5
10
15
20
Number of Prongs
PRONG DISTRIBUTION FOR EVENTS IN GAS OF CHAMBER NUMBER 1
Number of Events
0
5
10
15
20
Number of Prongs
PRONG DISTRIBUTION FOR EVENTS BETWEEN TARGET AND CHAMBER
Number of Events
0
5
10
Number of Prongs
XBL 736-788

Fig. 6

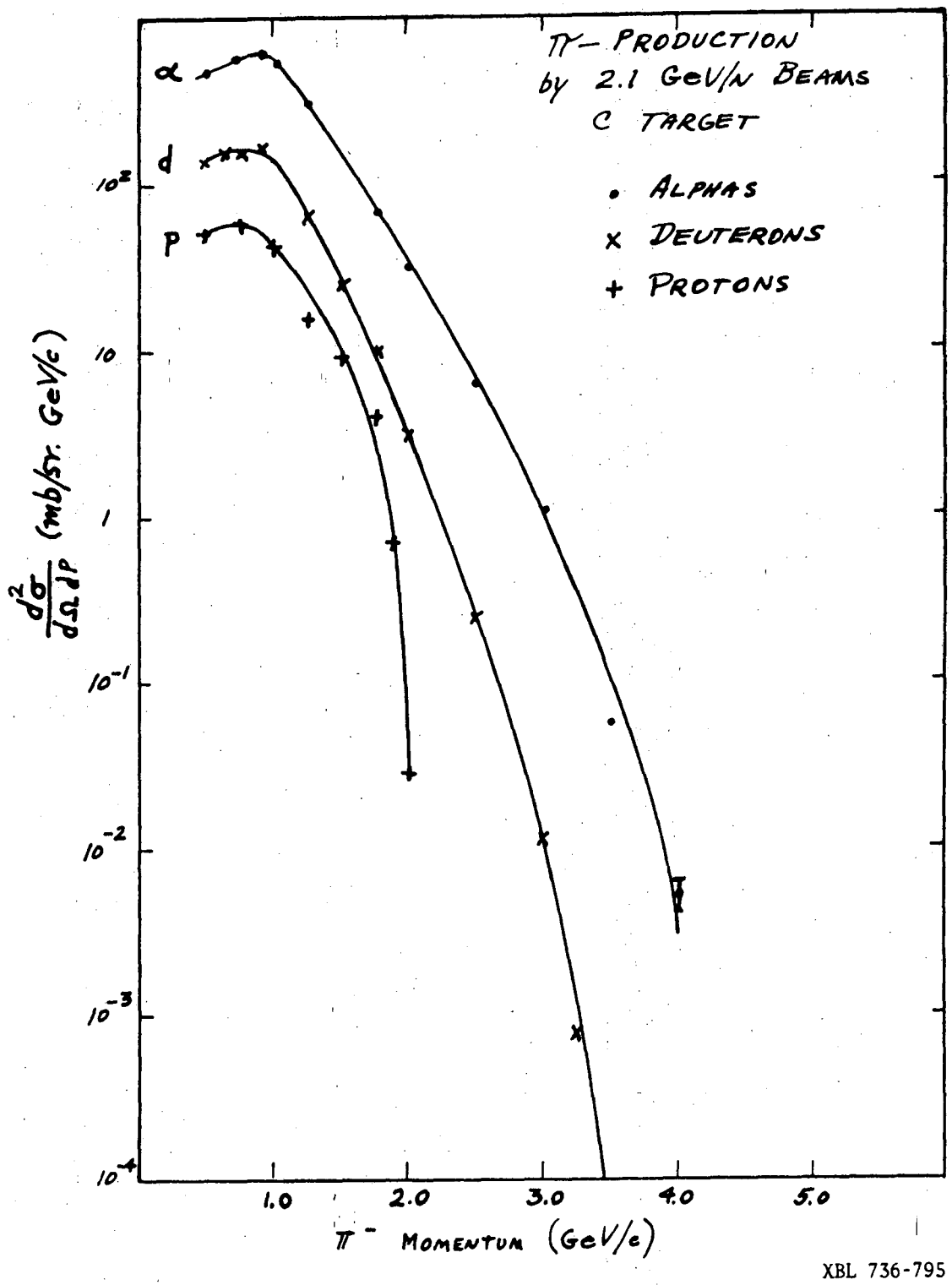

XBL 736-795

Fig. 7

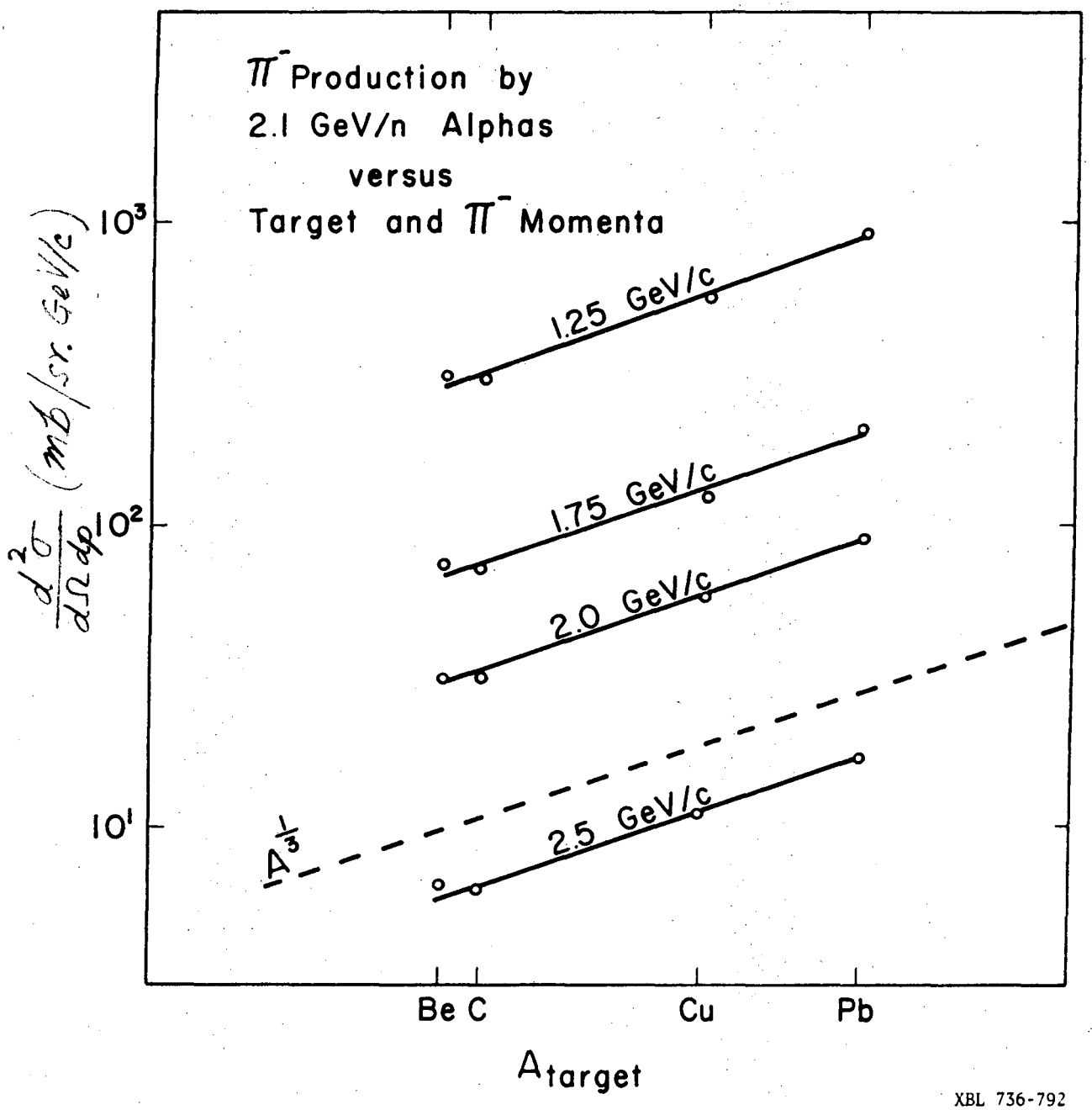
π⁻ Production by
2.1 GeV/n Alphas
versus
Target and π⁻ Momenta
1.25 GeV/c
1.75 GeV/c
2.0 GeV/c
2.5 GeV/c
A^1/3
10³
10²
10¹
d²σ/dΩdp (mb/sr. GeV/c)
Be C
Cu
Pb
A target
XBL 736-792

Fig. 8

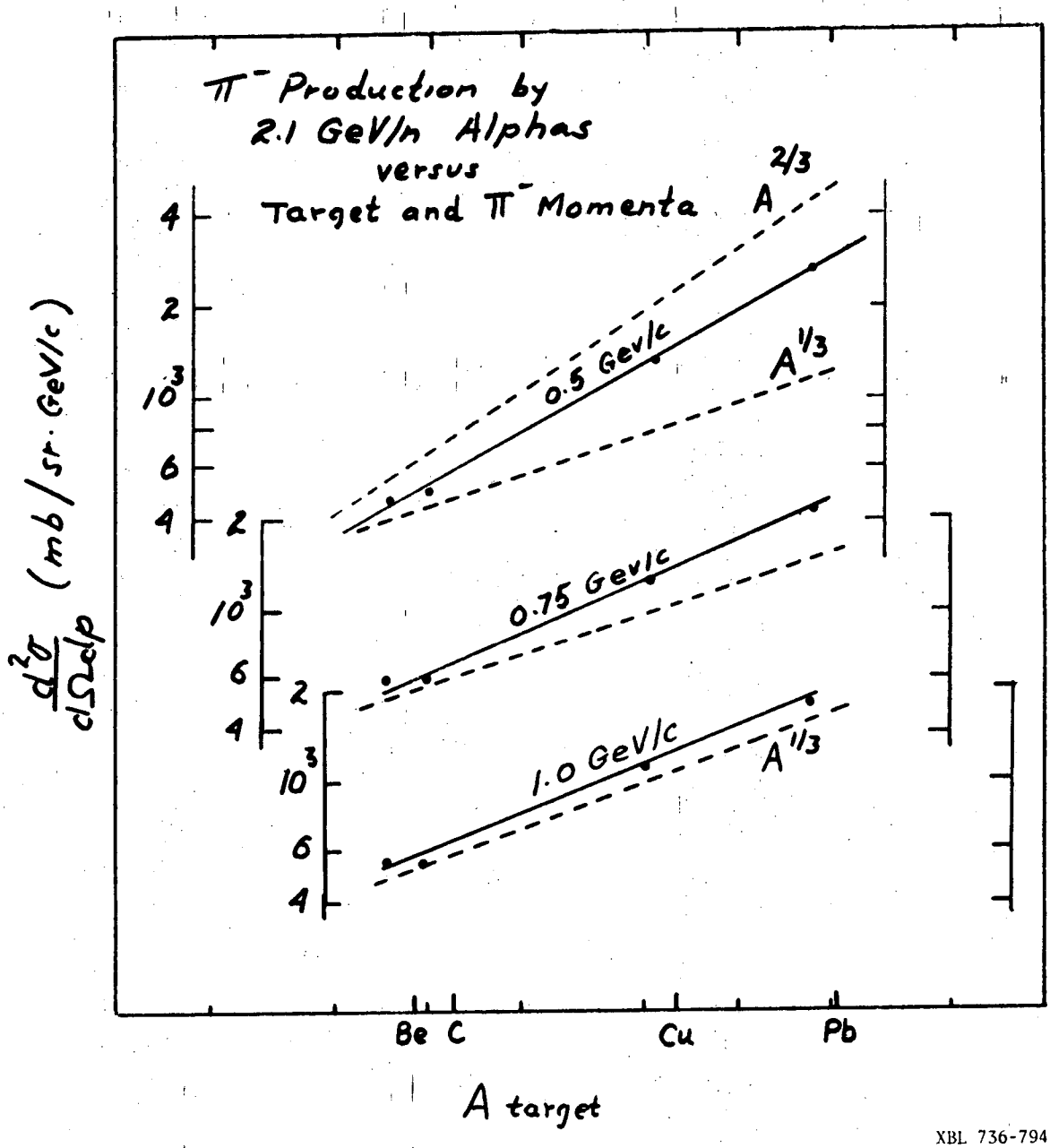

XBL 736-794

Fig. 9

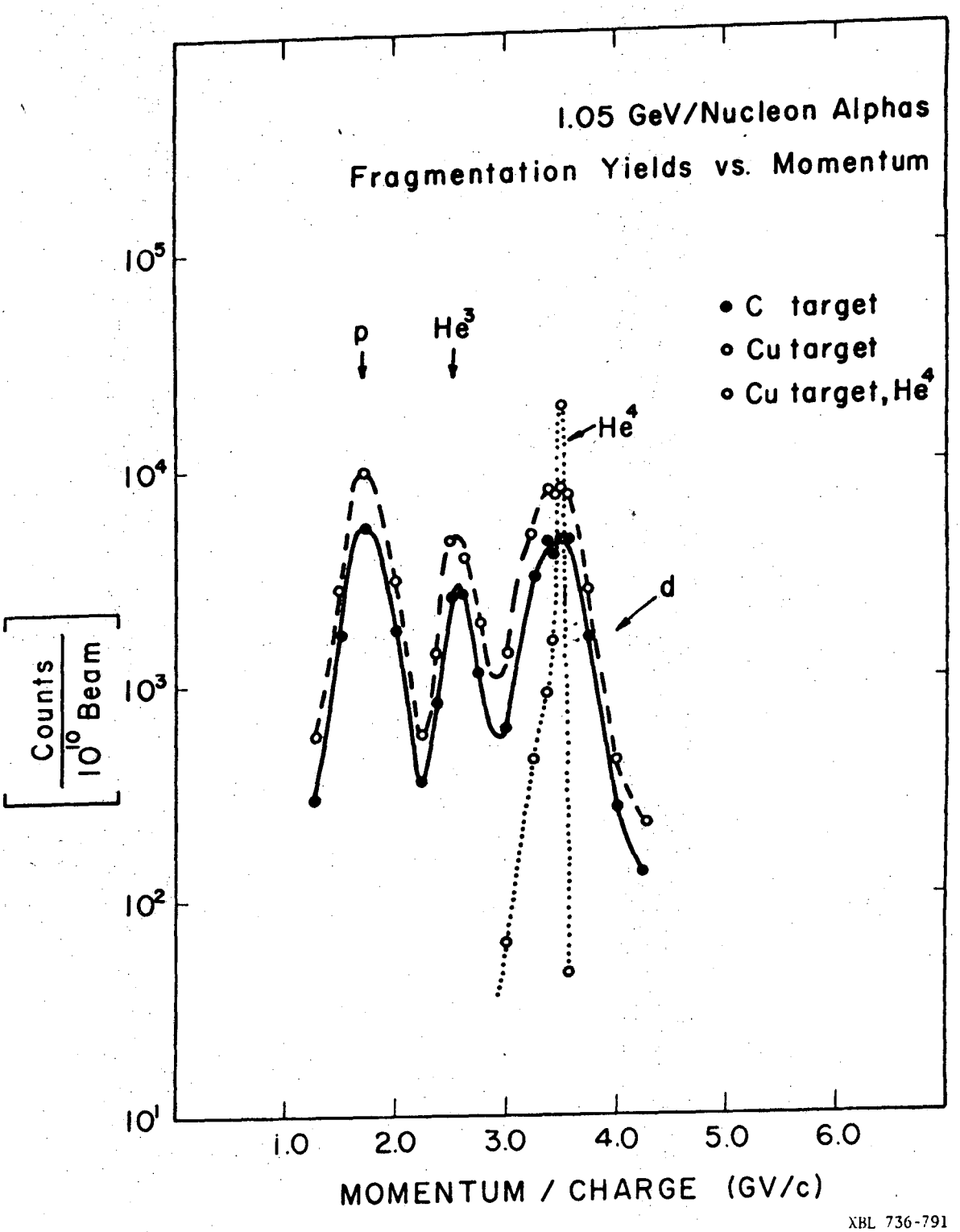
1.05 GeV/Nucleon Alphas
Fragmentation Yields vs. Momentum
C target
Cu target
Cu target, He4
p
He3
He4
d
Counts / 10^10 Beam
10^5
10^4
10^3
10^2
10^1
1.0
2.0
3.0
4.0
5.0
6.0
MOMENTUM / CHARGE (GV/c)
XBL 736-791

Fig. 10

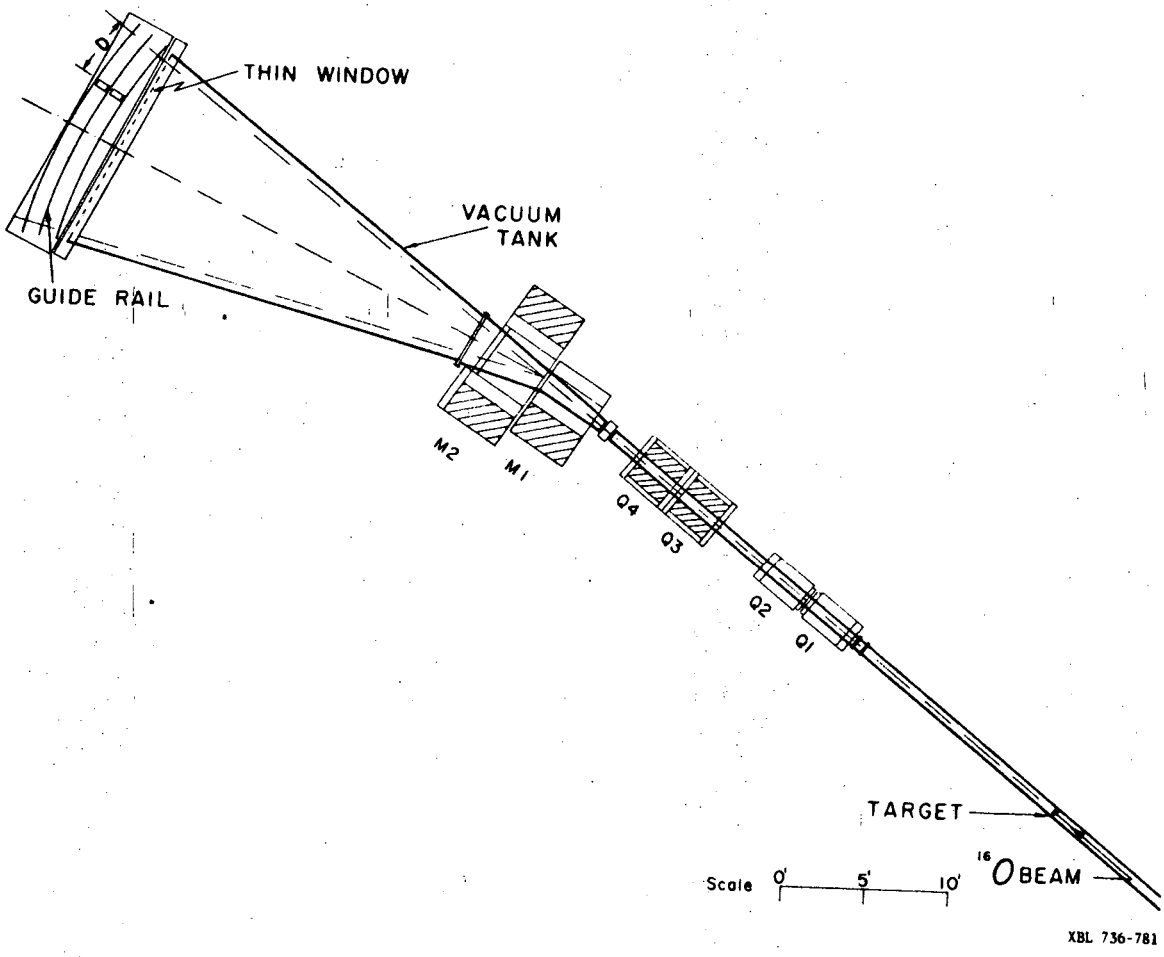
D1
THIN WINDOW
VACUUM TANK
GUIDE RAIL
M2
M1
Q4
Q3
Q2
Q1
TARGET
Scale 0' 5' 10'
16O BEAM
XBL 736-781

Fig. 11

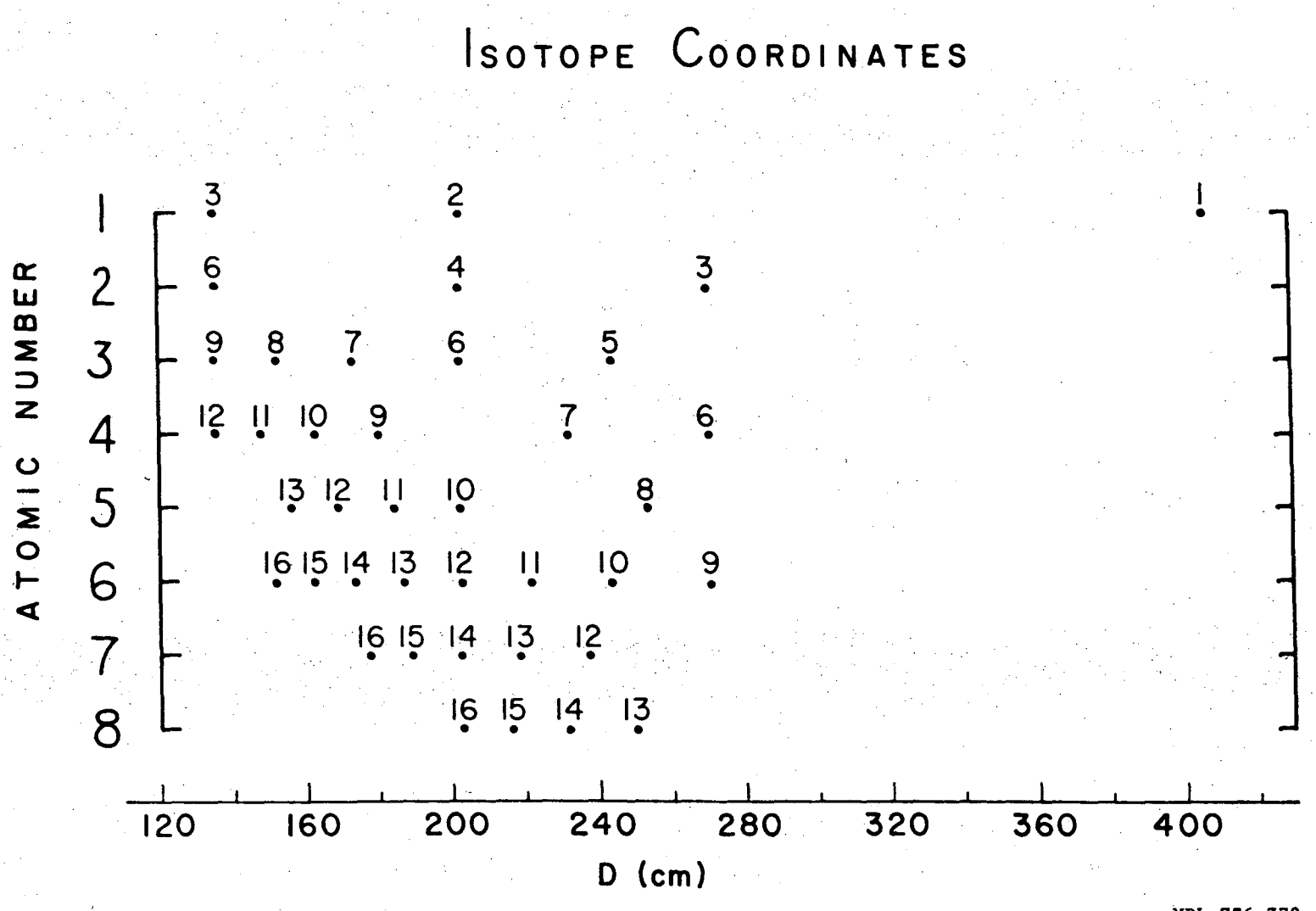
Isotope Coordinates
ATOMIC NUMBER
1
2
3
4
5
6
7
8
3
2
1
6
4
3
9
8
7
6
5
12
11
10
9
7
6
13
12
11
10
8
16
15
14
13
12
11
10
9
16
15
14
13
12
16
15
14
13
120
160
200
240
280
320
360
400
D (cm)
XBL 736-778

Fig. 12

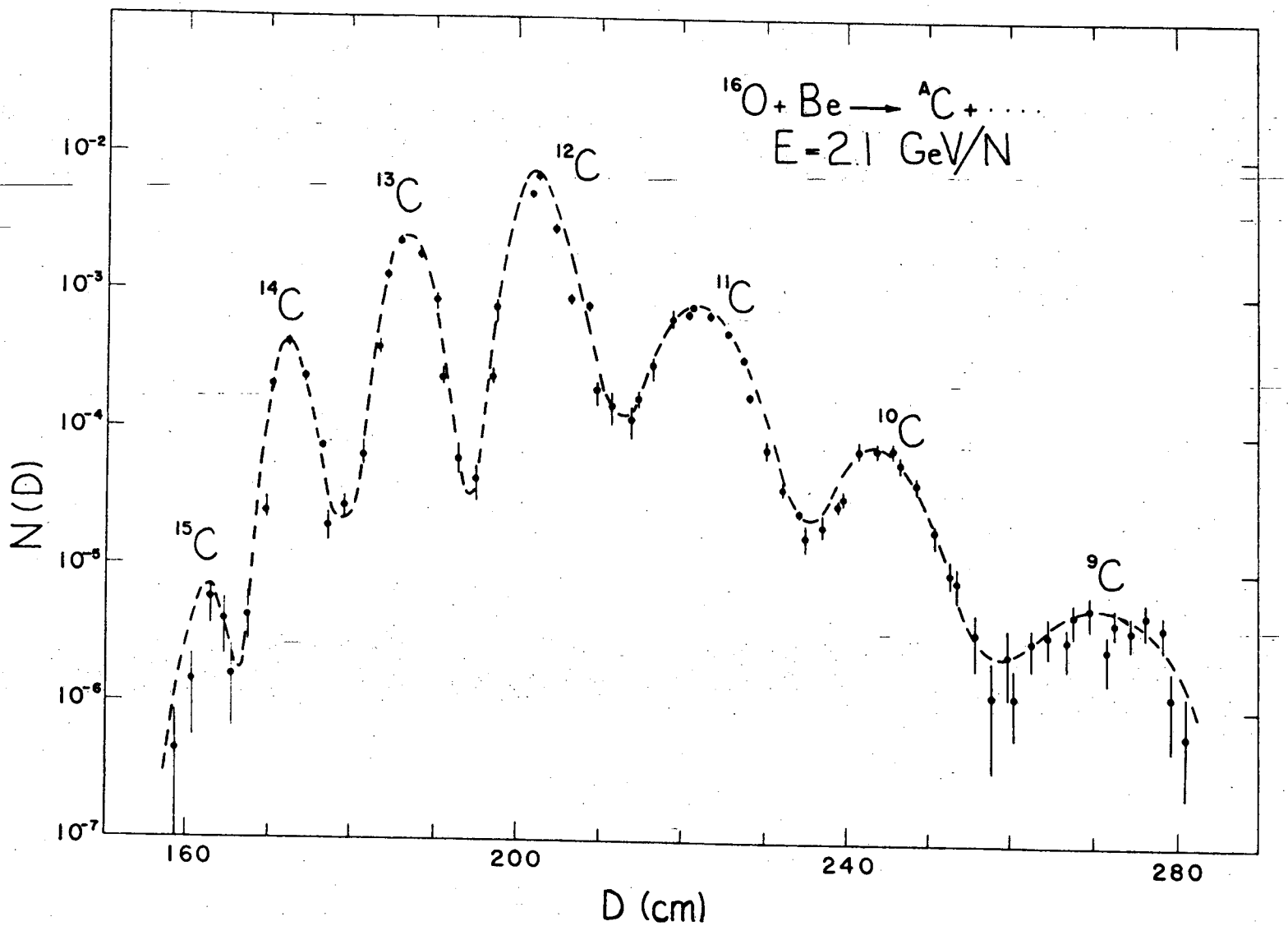

XBL 736-783

Fig. 13

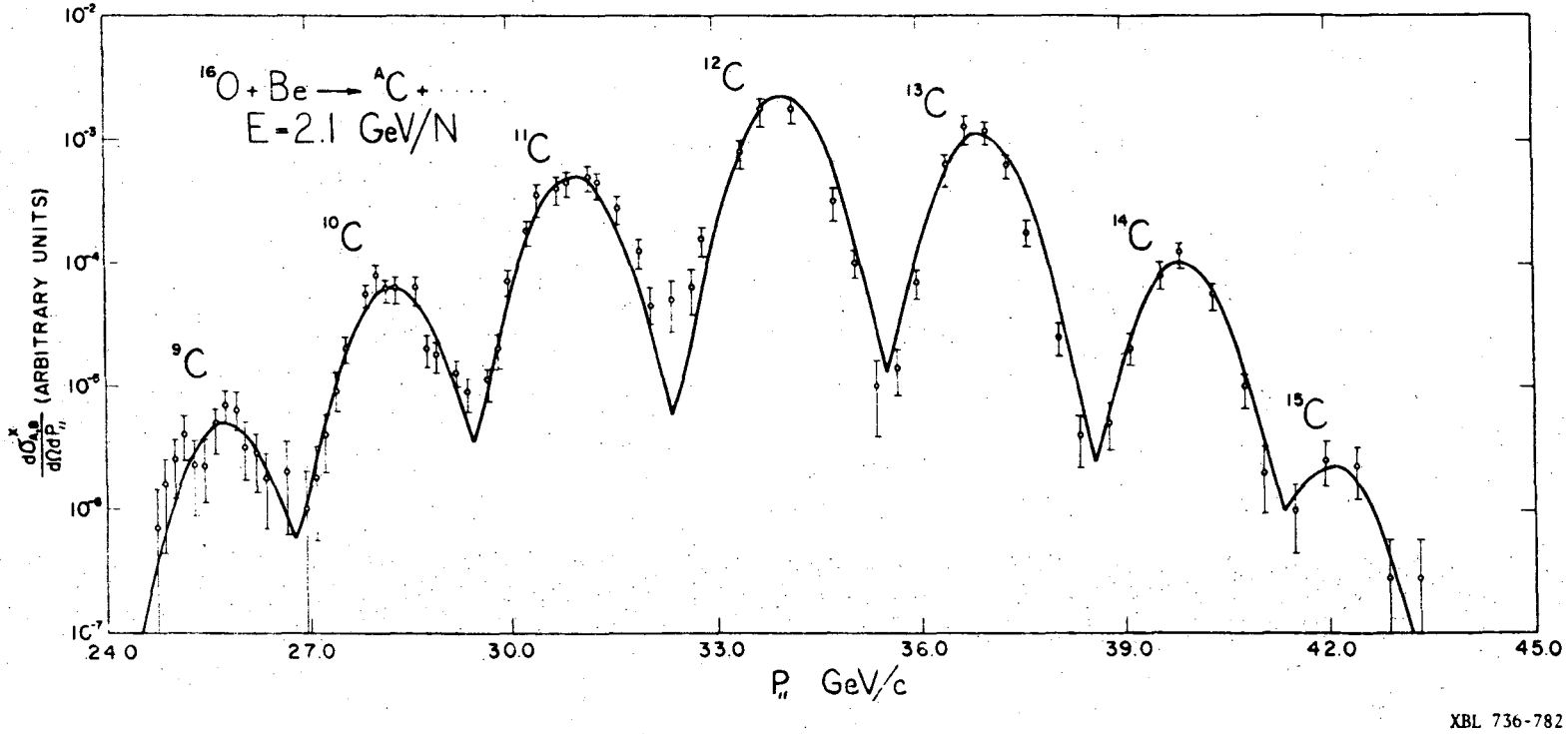
$^{16}O + Be \rightarrow {}^{A}C + \cdots$
E = 2.1 GeV/N
^{9}C
^{10}C
^{11}C
^{12}C
^{13}C
^{14}C
^{15}C
$\frac{d\sigma^{*}_{A,Z}}{d\Omega dP_{\parallel}}$ (ARBITRARY UNITS)
10^{-2}
10^{-3}
10^{-4}
10^{-5}
10^{-6}
10^{-7}
24.0
27.0
30.0
33.0
36.0
39.0
42.0
45.0
$P_{\parallel}$ GeV/c
XBL 736-782

Fig. 14

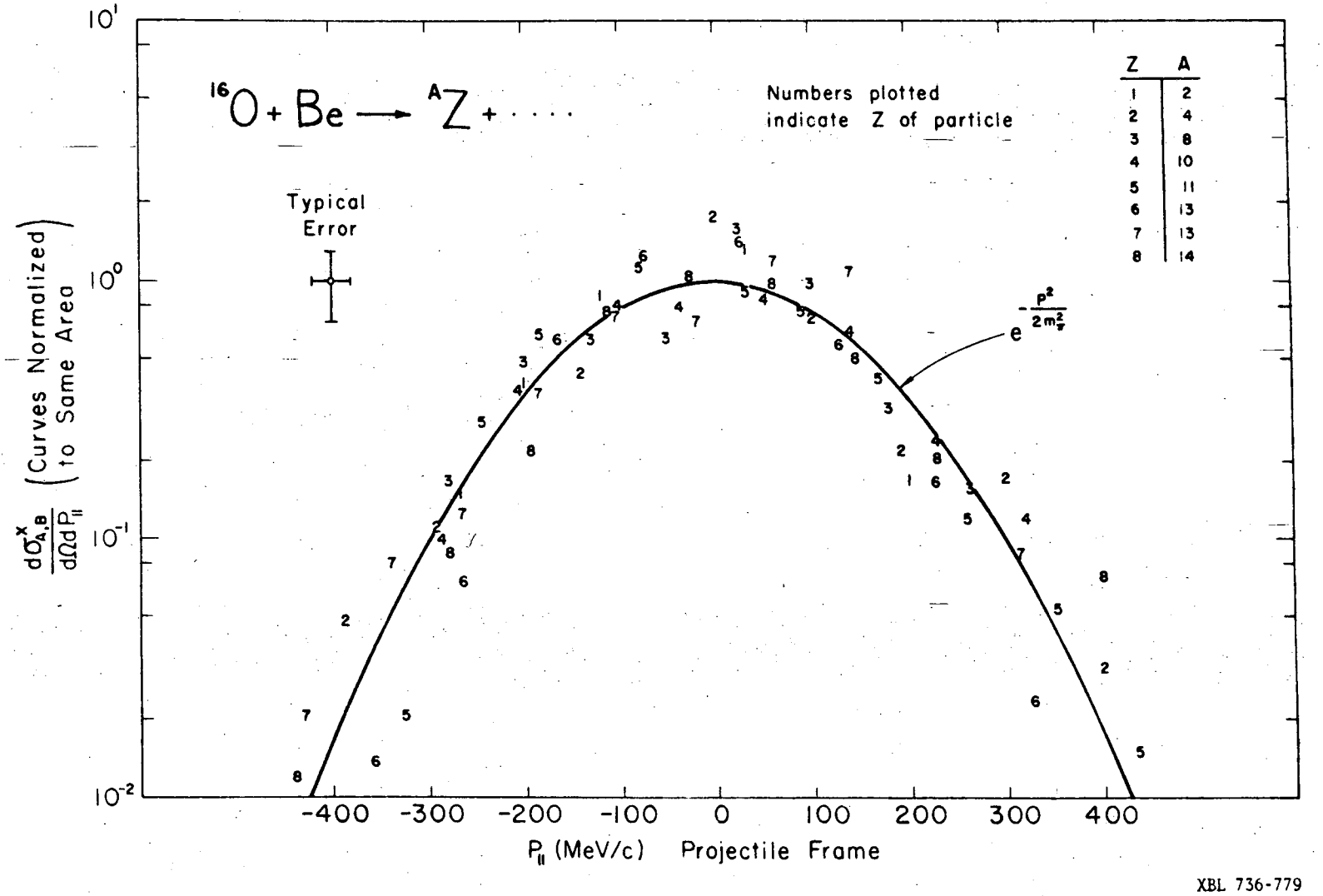
$^{16}O + Be \rightarrow {}^{A}Z + \cdots$
Numbers plotted indicate Z of particle
Z A
1 2
2 4
3 8
4 10
5 11
6 13
7 13
8 14
Typical Error
$e^{-\frac{p^2}{2m_z^2}}$
$\frac{d\sigma^{x}_{A,B}}{d\Omega dP_{\parallel}}$ (Curves Normalized to Same Area)
10^{1}
10^{0}
10^{-1}
10^{-2}
-400 -300 -200 -100 0 100 200 300 400
$P_{\parallel}$ (MeV/c) Projectile Frame
XBL 736-779

Fig. 15

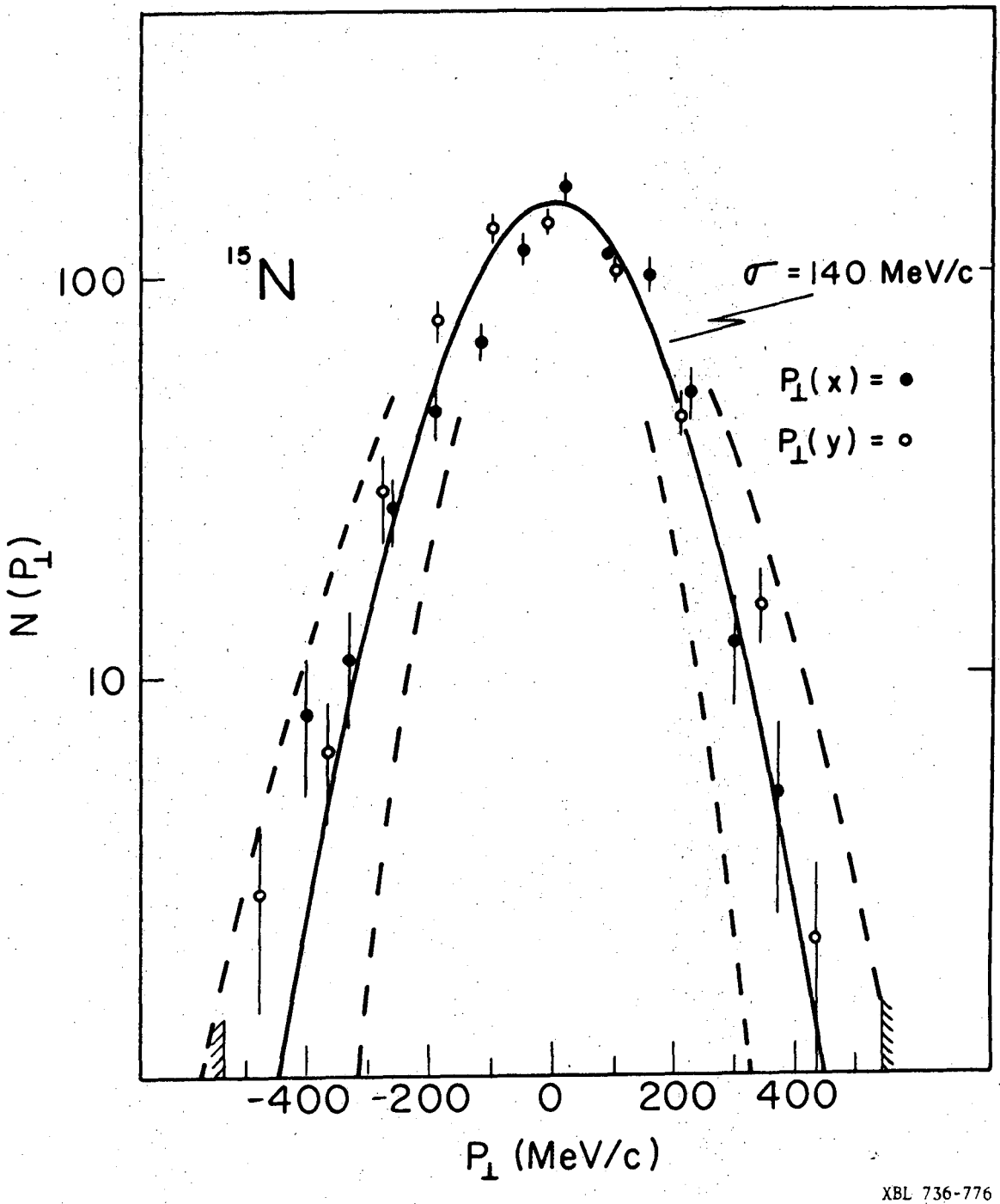

Fig. 16
(a)

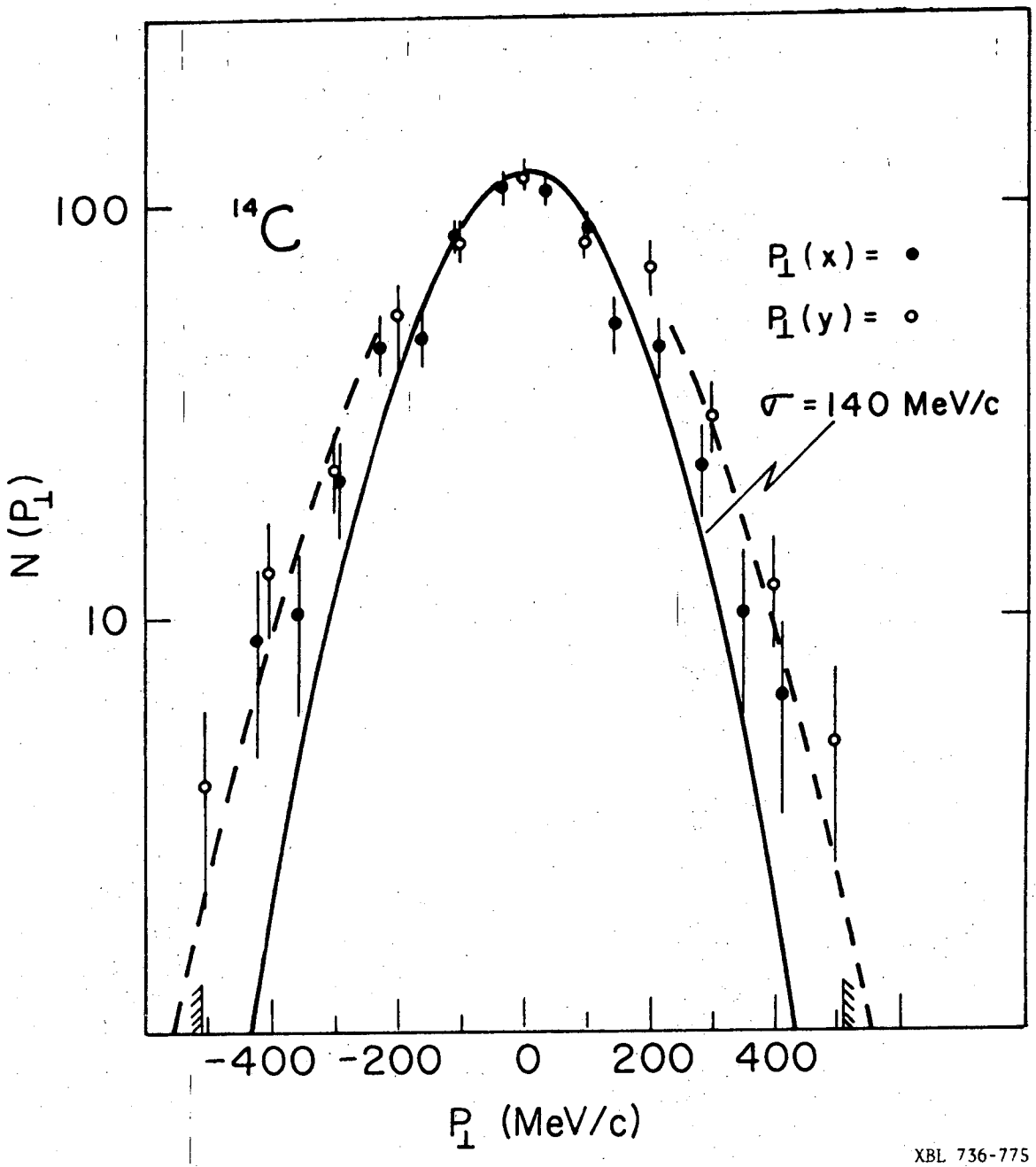
100
10
^{14}C
$P_\perp(x)$ = ●
$P_\perp(y)$ = ○
σ = 140 MeV/c
N ($P_\perp$)
-400 -200 0 200 400
$P_\perp$ (MeV/c)
XBL 736-775

Fig. 16
(b)

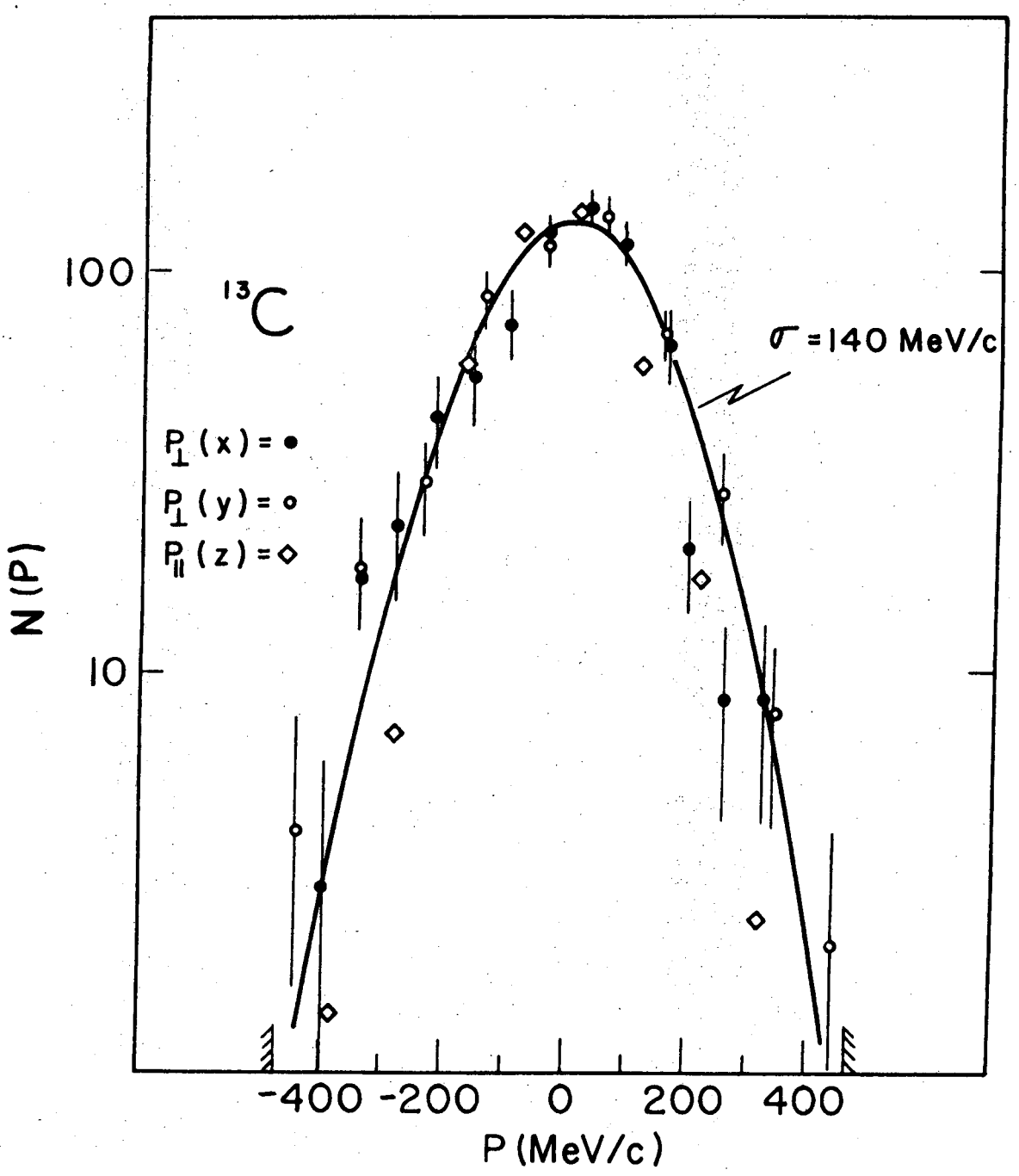
100
10
N(P)
^{13}C
σ = 140 MeV/c
$P_\perp(x)$ = ●
$P_\perp(y)$ = ○
$P_\parallel(z)$ = ◇
-400 -200 0 200 400
P (MeV/c)
XBL 736-777

Fig. 16
(c)

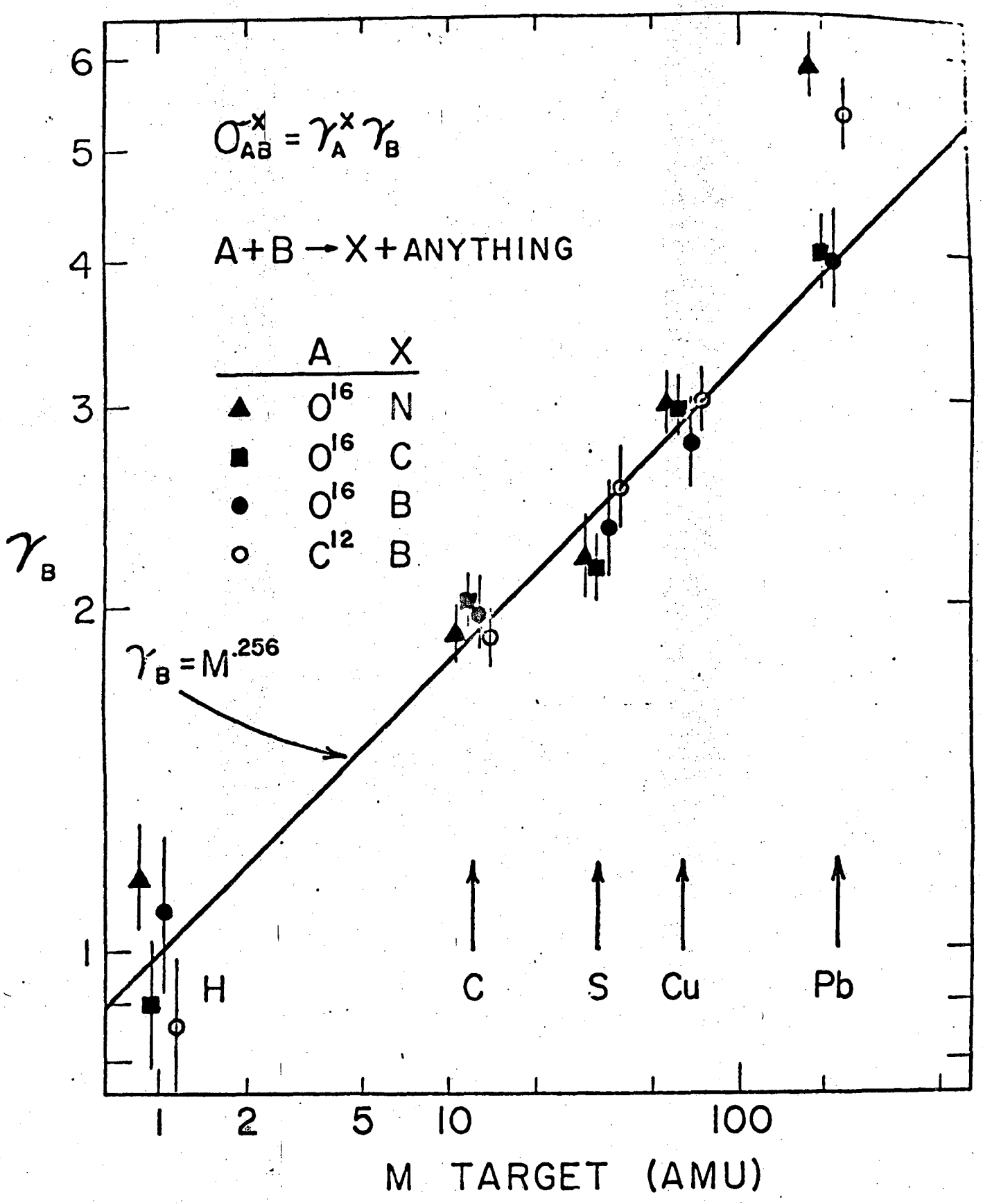
$\sigma_{AB}^{X} = \gamma_A^X \gamma_B$
A+B → X+ANYTHING
A X
▲ O^{16} N
■ O^{16} C
● O^{16} B
○ C^{12} B
γ_B
$\gamma_B = M^{.256}$
H
C
S
Cu
Pb
1
2
5
10
100
M TARGET (AMU)

Fig. 17

TECHNICAL INFORMATION DIVISION
LAWRENCE BERKELEY LABORATORY
UNIVERSITY OF CALIFORNIA
BERKELEY, CALIFORNIA 94720